New Zealand Journal of Geology & Geophysics, 2008, Vol. 51: 29–42
0028–8306/08/5101–0029

Ultra-fast early Miocene exhumation of Cavalli Seamount, Northland Plateau, Southwest Pacific Ocean

N. MORTIMER
GNS Science
Private Bag 1930
Dunedin 9054, New Zealand
n.mortimer@gns.cri.nz

W. J. DUNLAP
Research School of Earth Sciences
Australian National University
Canberra, ACT 0200, Australia
Present address Department of Geology & Geophysics, University of Minnesota, Minneapolis MN 55455, USA

J. M. PALIN
Department of Geology
University of Otago
PO Box 56
Dunedin 9054, New Zealand

R. H. HERZER
GNS Science
PO Box 30368
Lower Hutt 5040, New Zealand

F. HAUFF
IFM-GEOMAR Leibniz Institute for Marine Sciences
Wischhofstrasse 1-3
D-24148 Kiel, Germany

M. CLARK
NIWA
Private Bag 14901
Kilbirnie, Wellington 6241, New Zealand

Abstract We present new photographic, petrological, geochronological, and isotopic data for gneissic and granitic rocks obtained from six sample stations on Cavalli Seamount during two cruises in 2002. These data lead to revision of earlier conclusions based on two dredges of schist in 1999. Based on c. 100 Ma ages of zircon cores, and whole rock petrochemistry and tracer isotopes, we interpret the protoliths of paragneisses and orthogneisses to probably have been sedimentary and plutonic correlatives of the Late Cretaceous Houhora Complex. U-Pb dating of low Th/U zircon rims confirms an earliest Miocene high-grade metamorphic episode. A cooling history based on Ar-Ar K-feldspar dating indicates ultra-rapid cooling (c. 2000°C/m.y.) and vertical exhumation (c. 100 mm/yr) of the rocks at 19.9 Ma. Our preferred tectonic model relates the amphibolite facies metamorphism to Northland Allochthon emplacement and the rapid exhumation to dextral transtension along the Vening Meinesz Fracture Zone system and/or a rapidly retreating Pacific trench.

Keywords New Zealand; Southwest Pacific Ocean; Northland Plateau; Vening Meinesz Fracture Zone; Northland Allochthon; tectonics; exhumation; strike-slip faulting; geochronology; Miocene

G07013; Online publication date 28 February 2008
Received 28 June 2007; accepted 18 December 2007

INTRODUCTION

Cavalli Seamount is a prominent, flat-topped, c. 40 × 20 × 1 km feature located c. 100 km ENE of North Cape (Fig. 1, 2) (Mitchell & Eade 1990). Geomorphically it lies off the well-defined Northland continental slope, near the edge of the Northland Plateau (Herzer et al. 2000). In a cruise in 1999, samples of schist were recovered from two dredges on the east slopes of Cavalli Seamount. Post-cruise analysis and interpretation of those rocks led Mortimer et al. (2003) to propose a Miocene metamorphic core complex model. Key results leading to this model were establishment of (1) Late Cretaceous–Paleogene sedimentary protolith and (2) rapid early Miocene exhumation.

This paper is an update of Mortimer et al. (2003) and is based on new, previously unpublished results from two cruises made in 2002 (Clark et al. 2002; Herzer et al. 2004) (Table 1). One, a dedicated geological cruise by GNS Science, made one rock dredge up the south flank of the western part of Cavalli. On a separate biological cruise by the National Institute of Water and Atmospheric Research (NIWA), rocks were recovered as "by-catch" at several stations on the seamount's flat top, and bottom camera traverses were made of the seabed. Our new samples, analyses, and images give more confidence to, and supplement, the interpretations made by Mortimer et al. (2003).

With the publication of dredging results from the Northland Plateau (Mortimer et al. 2007), it is now possible to view Cavalli in an onland-offshore geological context (Fig. 1). Much of the Northland continental shelf edge (<1500 m water depth) is underlain by the Vening Meinesz Fracture Zone (VMFZ) system of faults. Cavalli Seamount and the Northland Plateau (a broad region of mainly Miocene volcanoes) lie between the VMFZ and the edge of the Kupe Abyssal Plain of the South Fiji Basin (c. 3000 m water depth). Cavalli Seamount separates the Knights and Whangaroa Basins. The autochthonous basement geology of onland Northland comprises Waipapa Terrane (Permian–Jurassic greywacke-argillite association with minor basalt-chert-limestone) and Houhora Complex (Late Cretaceous intercalated submarine basalt, andesite, dacite, rhyolite, tuff-breccia, conglomerate, sandstone, and mudstone) (Isaac et al. 1994; Isaac 1996). Houhora Complex igneous rocks have given U-Pb zircon ages of c. 102 Ma (GNS unpubl. data). Late Cretaceous–Oligocene sedimentary rocks rest unconformably on the basement.

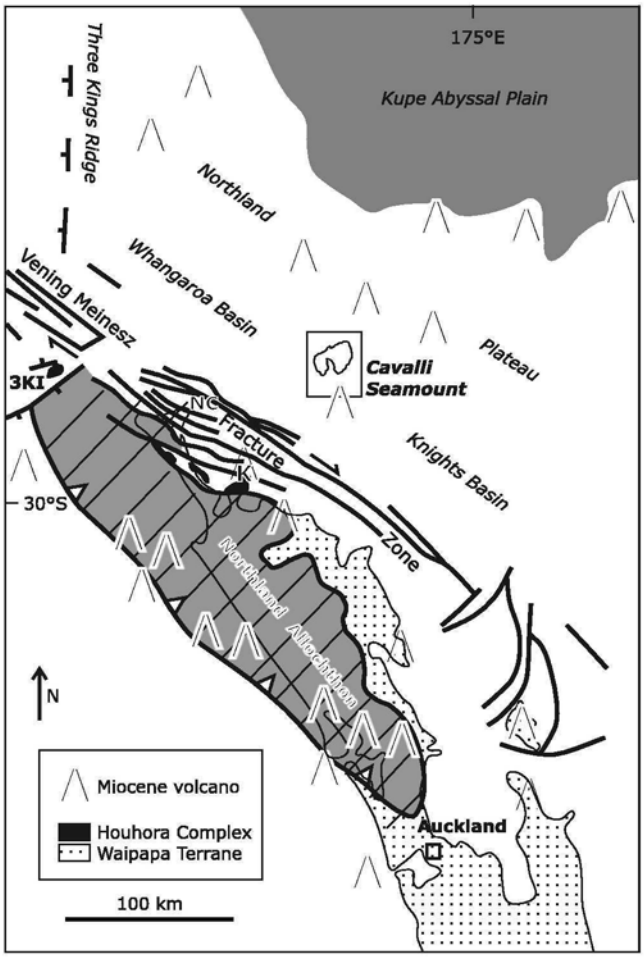

Fig. 1 Location of Cavalli Seamount (1200 m isobath shown) in relation to neighbouring geological features of onland and offshore Northland. Only onshore and western parts of the allochthon are shown. Late Cretaceous–Pleistocene sedimentary cover are not shown. 3KI = Three Kings Islands, NC = North Cape, K = Karikari Peninsula. Rectangle is area of Fig. 2. After Isaac et al. (1994), Herzer & Mascle (1996), and Mortimer et al. (2007).

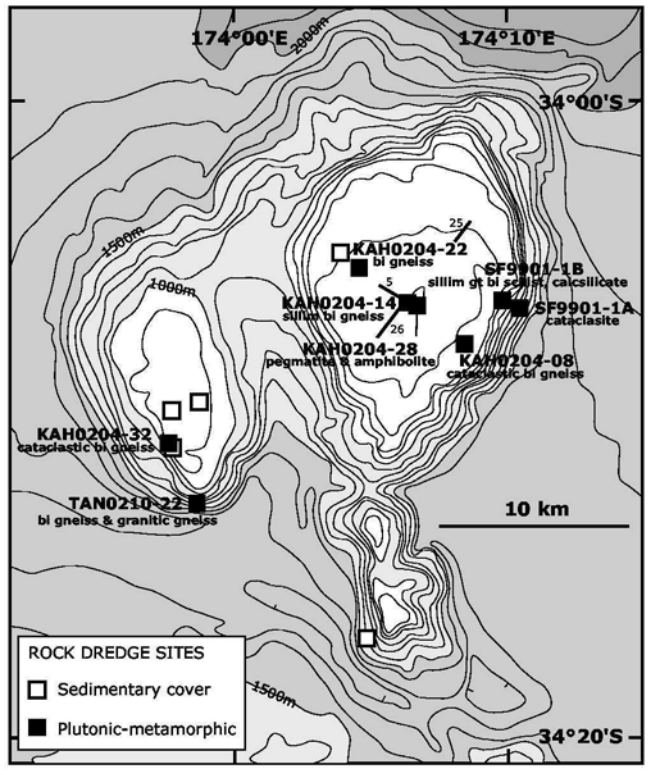

Fig. 2 Location of dredge sites, and plutonic-metamorphic rock types obtained from Cavalli Seamount on GNS *Tangaroa* cruises SF9901 and TAN0210, and on NIWA *Kaharoa* cruise KAH0204. *Kaharoa* camera station tracks 5 and 25 also shown. Bathymetry from Mitchell & Eade (1990). For sample details see Table 1.

Tectonically overlying the autochthonous rocks is a now-southwest-tilted thrust sheet, the Northland Allochthon, which was emplaced in the Waitakian (early Miocene, 25–22 Ma). Following allochthon emplacement, early Miocene volcanoes of the Northland Arc erupted through and onto the allochthon and, probably in the same early-middle Miocene time interval, the dextral VMFZ juxtaposed rocks of the Northland Plateau, including Cavalli Seamount, against the Northland continental margin (Fig. 1).

METHODS

With a few exceptions, X-ray fluorescence (XRF), inductively coupled plasma mass spectrometry (ICP-MS), Ar-Ar and U-Pb dating, and Sr, Nd and Pb isotopic analytical methods are identical to those reported in Mortimer et al. (2006, appendix DR1). After analysing the whole rocks by ICP-MS with acid dissolution, it was realised that there were unrealistically low concentrations of Zr and rare-earth elements, presumably due to incomplete sample dissolution of minerals such as zircon. Samples were thus reanalysed by ICP-MS using fused bead dissolution, as indicated in Table 2. The analytical approach used in $^{40}Ar/^{39}Ar$ analysis is identical to that outlined in Dunlap (2003), except for the following: correction factors used are $(^{37}Ar/^{39}Ar)_{Ca} = 3.50 \times 10^{-4}$, $(^{39}Ar/^{37}Ar)_{Ca} = 7.86 \times 10^{-4}$, $(^{40}Ar/^{39}Ar)_{K} = 0.027$. The individual step ages of the K-feldspar were calculated using the Fish Canyon sanidine neutron fluence (dose) monitor, which has an intercalibrated age of 28.1 ± 0.04 Ma (Spell & McDougall 2003).

All samples have been lodged in the GNS Petrology "P" Collection, and associated sample and analytical data have been catalogued in the PETLAB database (http://pet.gns.cri.nz).

SAMPLE DATA

During the KAH0204 cruise, 317 photographs were taken during the course of 11 still-camera tows across the tops of the eastern and western parts of Cavalli Seamount. In most cases the camera faced vertically down, perpendicular to the seafloor. The camera was not deliberately oriented, the purpose being to take biological images. We believe that the long axis of the photographs was probably oriented parallel to the ship's track, although the possibility of cross-currents and local sled disturbances means we cannot be entirely sure of this. *In situ* rock exposures (as opposed to sandy or muddy bottom) were visible in about one-fifth of the photographs, and 21 photographs in nine different tows showed a significant

Table 1 Sample location and description data for Cavalli samples dredged in 1999 and 2002.

GNS P#	Deck#	Sample size	Rock names	Notes
SF9901-1A, 23 Mar 99, –34.1050S, 174.1781E, 985–1229 m				
63144-48	D1A-1-4	<1 kg	cataclastic schist	See Mortimer et al. (2003).
SF9901-1B, 23 Mar 99, –34.1005S, 174.1668E, 577–778 m				
62586, 62656–65, 63139–63143		>100kg	gt bi schist and calcsilicate gneiss	See Mortimer et al. (2003).
KAH0204-08, 14 Apr 02, –34.1152S, 174.1450E, 610–640 m				
67667	D8-1	30×20×20 cm angular with broken face	cataclastic biotite schist/gneiss	Cataclastic textures prominent. Biotite retrograded to chlorite. Faults grade into open cracks with calcooze infilling.
KAH0204-14, 15 Apr 02, –34.0957S, 174.1105E, 507–520 m				
67670	D14-1	35×25×10 cm slab	biotite paragneiss and orthogneiss	Fine-grained biotite gneiss in contact with coarser perthitic biotite gneiss.
67671	D14-2	20×15×10 cm angular, irregular	sillimanite biotite paragneiss	Quartz, oligoclase, biotite, garnet, sillimanite, FeTi oxide, titanite, muscovite.
KAH0204-22, 16 Apr 02, –34.078S, 174.0787E, 550–610 m				
67673*	D22-1	15×10×7 cm, angular with broken face	granodioritic orthogneiss	Weakly foliated. Granodioritic composition from geochemistry.
67674	D22-2	20×20×7 cm angular	granodioritic orthogneiss	Weakly foliated. Identical to P67670.
KAH0204-28, 16 Apr 02, –34.0963S, 174.1148E, 490–515 m				
67676	D28-1	10×7×4 cm subangular block	pegmatite and amphibolite	Garnet hornblendite (inclusion?) in contact with (larger mass of?) granite pegmatite, median grain size 8 mm.
KAH0204-32, 17 Apr 02, –34.1620S, 173.9618E, 780–810 m				
67678*	D32-1	4×3×2 cm angular	cataclastic biotite paragneiss	Grey-green hard rebrecciated and sediment-cemented cataclastic gneiss.
TAN0210-22, 5 Aug 02, –34.2070S, 173.9784E, 1330–1750 m				
66836	D22-1A	5–50 cm subangular boulder	banded biotite paragneiss	20% quartz, 60% oligoclase, 15% biotite, 5% anhedral garnet, FeTi oxide, titanite, graphite, apatite 0.3 mm median grain size. Cut by 1 cm irregular veins of granitic gneiss (see P66839) that are subparallel to, and crosscut but predate, the main foliation.
66837	D22-1B	5–50 cm subangular boulder	banded biotite paragneiss	Similar to P66836 but with mica segregations spaced at 5 mm. Biotite is more oxidised. Granitic veins are more intimately interbanded and the whole rock analysis is probbaly a mix of host gneiss and granite.
66838	D22-1C	5–50 cm subangular boulder	migmatitic gneiss	Up to half of sample is irregular granitic veins. Forams in crack infill.
66839	D22-2A	40×30×20 cm angular slab	granitic orthogneiss	50% quartz, 20% K-feldspar, 25% plagioclase, 5% chloritised biotite, FeTi oxides, secondary muscovite. Weakly foliated.
66840	D22-2B	5–50 cm subangular boulder	folded, veined biotite gneiss	Similar to P66838. Irregular (pytgmatic, pre-main foliation) granitic veins up to 2 cm wide cut gneiss. Accessory tourmaline in one granitic vein.
66841	D22-3	5–20 cm bored subrounded slab	soft sandy mudstone	Bioturbated, foram-bearing, some gneissic clasts.
66842	D22-4	5–20 cm bored subrounded slab	hard brown sandstone	Some gneissic clasts.

*No thin section: hand sample description only.

Table 2 Whole rock analyses of Cavalli samples dredged in 2002.

GNS P#	P66836	P66837	P66839	P67673	P67674
Dredge	SF0202-22	SF0202-22	SF0202-22	KAH0204-22	KAH0204-22
rock	biotite paragneiss	biotite and granite gneiss	granitic orthogneiss	granodioritic orthogneiss	granodioritic orthogneiss
SiO_2 (wt%)	66.27	71.22	73.79	64.01	62.69
TiO_2	0.67	0.64	0.10	0.56	0.61
Al_2O_3	17.19	14.22	14.84	15.20	15.38
Fe_2O_3T	3.51	4.88	0.70	4.04	4.42
MnO	0.07	0.06	0.01	0.07	0.07
MgO	1.22	1.42	0.27	1.90	1.88
CaO	2.87	0.74	1.41	4.20	4.56
Na_2O	4.39	2.01	4.18	4.33	4.39
K_2O	2.64	2.83	3.94	2.68	3.01
P_2O_5	0.10	0.07	0.10	0.19	0.19
LOI	0.84	1.82	0.52	2.53	2.74
Total	99.77	99.90	99.86	99.69	99.94
As (ppm)	<1	3	1	<1	<1
Ba	1010	599	708	704	810
Ce	78.7	56.2	31.1	56.3	63.1
Co	na	50.5	76.9	71.4	59.3
Cr	21	44	<1	26	26
Cs	2.50	3.08	2.53	3.60	3.60
Cu	18	22	2	2	7
Dy	6.89	3.37	2.46	3.34	3.74
Er	4.03	1.98	1.32	1.86	2.09
Eu	1.47	0.688	0.227	0.907	0.953
Ga	22.7	18.98	17.9	19.6	20.8
Gd	7.17	3.89	2.69	4.07	4.39
Hf	7.91	7.52	2.58	5.09	7.11
Ho	1.39	0.709	0.473	0.649	0.732
La	34	24.4	15.4	27.4	30.8
Li	na	24.5	4.54	22.1	25.2
Lu	0.643	0.360	0.202	0.305	0.341
Mo	na	0.601	0.127	0.193	0.129
Nb	13.0	9.48	7.09	5.97	8.68
Nd	37.1	23.4	12.2	24.8	27.9
Ni	13	26	<2	19	15
Pb	30.1	15.6	26.8	17.9	16.9
Pr	9.55	6.32	3.46	6.76	7.53
Rb	93.9	102	128	89.3	95.6
Sb	na	0.184	0.093	0.043	0.054
Sc	11	12	<2	12	12
Sm	7.74	4.52	2.67	4.73	5.23
Sn	na	0.940	2.03	2.14	2.23
Sr	511	161	190	534	530
Ta	na	0.191	0.795	0.475	0.375
Tb	1.17	0.543	0.396	0.591	0.653
Th	11.9	10.6	7.77	9.47	10.7
Tl	na	0.731	0.632	0.581	0.653
Tm	0.609	0.309	0.199	0.280	0.317
U	3.22	2.31	2.90	1.71	2.07
V	57.8	83.3	8.46	69.9	76.7
Y	39.2	18.5	15.3	18.6	20.5
Yb	4.21	2.24	1.40	2.02	2.23
Zn	80.8	89.1	15.0	64.7	64.6
Zr	267	254	65	175	199
$^{87}Sr/^{86}Sr \pm 2\ \sigma$	0.708922	0.709483	0.706886	0.705913	0.705919
	0.000004	0.000004	0.000004	0.000004	0.000005
$^{143}Nd/^{144}Nd \pm 2\ \sigma$	0.512659	0.512471	0.512643	0.512553	0.512553
	0.000002	0.000002	0.000002	0.000002	0.000002
$^{206}Pb/^{204}Pb \pm 2\ \sigma$	18.833	18.839	18.833	18.841	18.838
	0.001	0.001	0.001	0.001	0.001
$^{207}Pb/^{204}Pb \pm 2\ \sigma$	15.628	15.629	15.619	15.621	15.615
	0.001	0.001	0.001	0.001	0.001
$^{208}Pb/^{204}Pb \pm 2\ \sigma$	38.736	38.758	38.707	38.798	38.780
	0.001	0.002	0.001	0.001	0.001

Major elements and As, Cr, Cu, Ni, Sc, and Zr by X-ray fluorescence methods at Spectrachem Analytical. Li, Co, Mo, Sb, Sn, Ta and Tl by ICP-MS dissolution methods at University of Kiel. All other elements by ICP-MS fused bead methods at University of Kiel. LOI = Loss on ignition, na = not analysed.

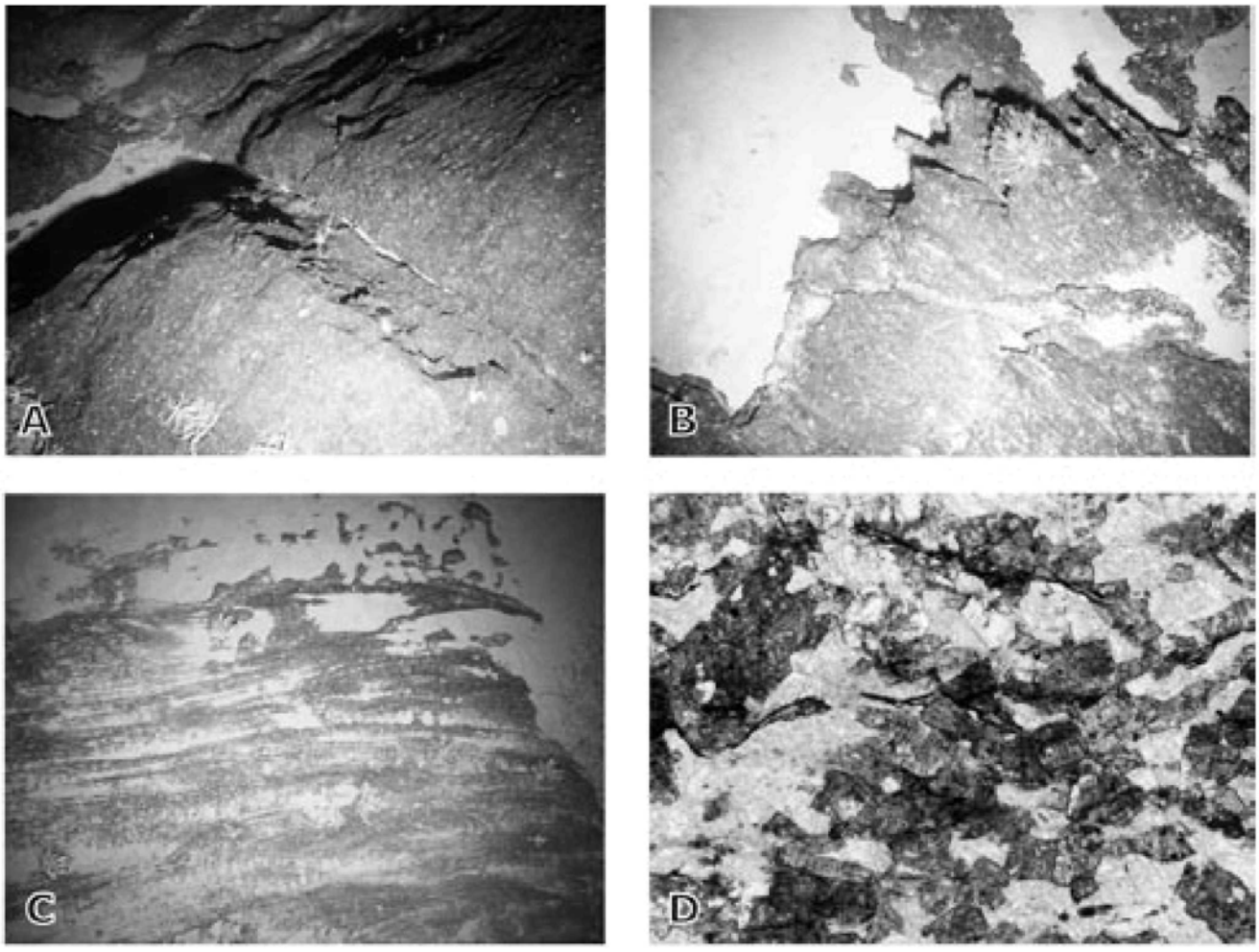

Fig. 3 KAH0204 camera images of Cavalli seafloor; field of view c. 2 m (see Fig. 2 for locations), inferred azimuths are speculative (see text for discussion). **A**, Station 5, photo 8928, showing moderately developed subhorizontal gneiss foliation cut by sediment-filled subvertical joint which possibly strikes 170. **B**, Station 25, photo 9351, showing well-developed subhorizontal gneiss foliation with a pronounced penetrative lineation that has a possible azimuth of 075. **C**, Station 26, photo 9369, showing rare subvertically dipping foliation with possible strike of 040. **D**, Microscope image of dated granitic orthogneiss P66839, 5 mm wide, taken in plane polarised light.

measure of photogeological detail. In most of these, the shadows cast by rock mass edges revealed the presence of a subhorizontally dipping planar anisotropic fabric, inferred to be metamorphic foliation (e.g,. Fig. 3A,B). In one case, steeply dipping, possibly isoclinally folded foliation appeared to be exposed on a subhorizontal joint face (Fig. 3C).

A summary of the hand specimen and petrographic characteristics of the igneous and metamorphic samples is given in Table 1. Including the two 1999 dredge sites, metamorphic and plutonic rocks have now been obtained from eight sample sites up to 20 km apart on the eastern and western parts of Cavalli Seamount (Fig. 2). In contrast to neighbouring seamounts on the Northland Plateau and continental shelf, which are extinct volcanoes (Fig. 1), it is significant that no volcanic or volcaniclastic rocks have thus far been obtained from Cavalli Seamount. This suggests that the entire seamount represents a significant submarine outcrop of continental metamorphic rocks.

Compared with the rocks dredged in 1999, no calcsilicate gneiss was sampled. The textures of the 2002 biotite-bearing metamorphic rocks are more semischistose-granoblastic than schistose, and have relatively poor fissility compared to the 1999 rocks. Hence, in the absence of mesoscopic field criteria, we describe the 2002 rocks as gneisses rather than schists (Compton 1985) but acknowledge there is probably a gradation between these rock types. The metamorphic mineral assemblages in the 2002 biotite gneisses are the same as in the 1999 biotite schists, with the index mineral sillimanite being present in gneiss P67671 from the eastern seamount top. Layering and heterogeneity probably indicates that most of the biotite gneisses had a metasedimentary protolith, and we refer to them as paragneisses.

Plutonic rocks were entirely absent from the two 1999 dredges. However, in the 2002 dredges, significant occurrences of metaplutonic rocks (granitic and dioritic gneiss) were discovered on both the eastern and western parts of the seamount (Fig. 2). These rock types occur both as deformed granitic veins in gneiss (e.g., P67670, P66838) and as separate boulders of granitic and dioritic gneiss (e.g., P66839). Foliation in the metaplutonic rocks is much weaker than in the aforementioned biotite gneisses, and banding is absent (Fig. 2). A sample of pegmatite vein cutting amphibolite (P67676) was obtained from the eastern top of the seamount.

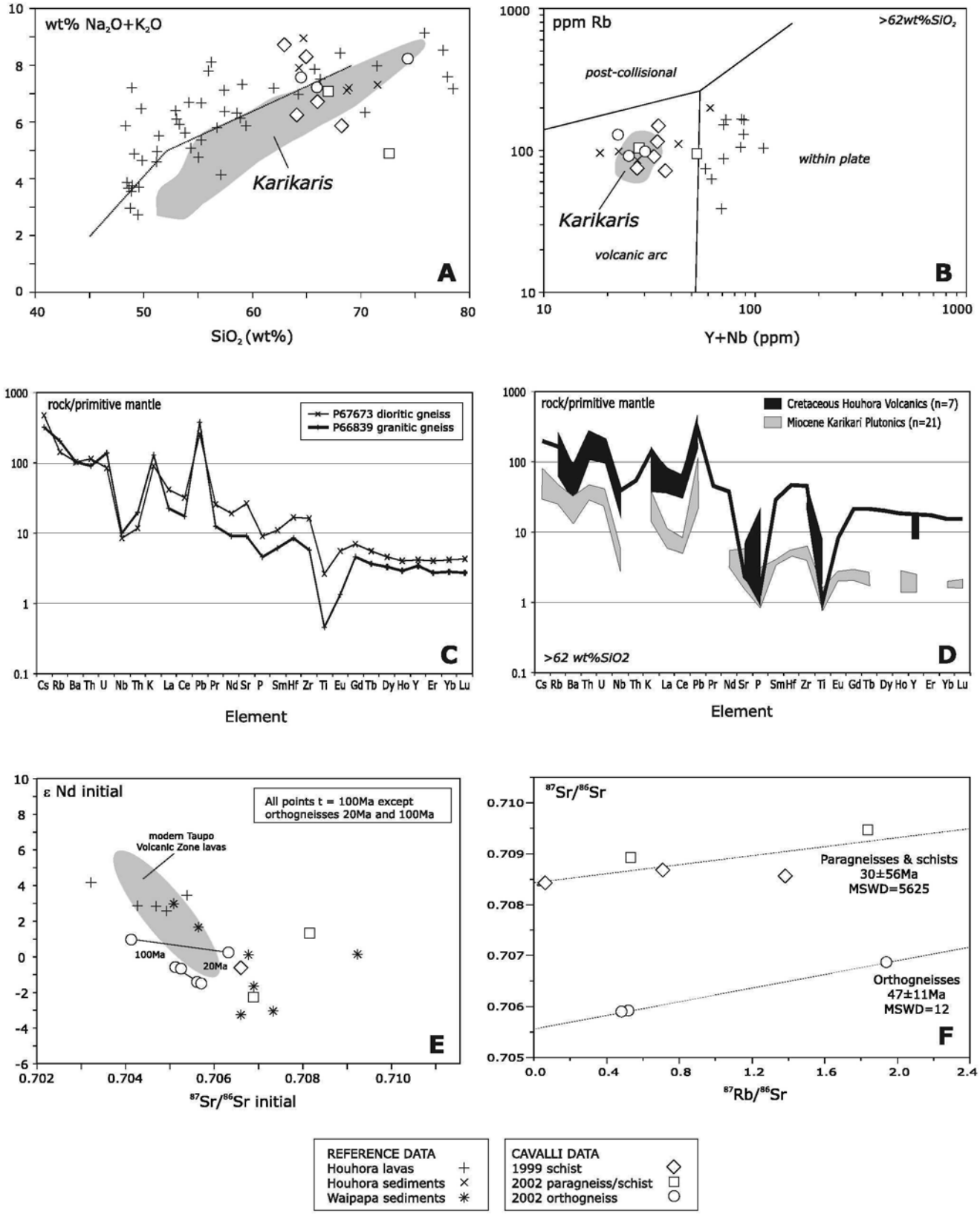

Fig. 4 Whole rock chemistry isotopic composition of Cavalli Seamount rocks compared with possible correlatives. **A**, Silica versus total alkalies diagram. **B**, Siliceous igneous rocks trace element diagram (Whalen et al. 1987). **C, D**, Primitive mantle normalised multi-element diagram (Sun & McDonough 1989). **E**, Sr versus Nd tracer isotope diagram. **F**, Strontium isochron diagram (no useful age information can be derived from the isochron lines, they are plotted for reference only). Reference data from Ruddock (1990), McCulloch et al. (1994), Palmer et al. (1995), Nicholson et al. (2000), Nicholson & Black (2004), Adams et al. (2005), and Mortimer et al. (1998, 2003, 2006).

ANALYTICAL DATA

Petrochemistry

Paragneisses

Mortimer et al. (2003) discussed the usefulness and limitations of petrography and of whole rock geochemical and isotopic analyses in helping correlate the metasedimentary rocks with specific geological units. Basically, the banded biotite gneisses in this study have broadly similar compositions to the 1999 biotite schists, but overall are slightly more silica-rich. Whole rock and tracer isotope data are compatible with any one of a number of local sources from Waipapa Terrane and Houhora Complex basement, to cover sequences eroded therefrom (Fig. 4). Dating of detrital zircons (see below) is more informative for stratigraphic correlation.

Orthogneisses

Three analyses of the weakly foliated metaplutonic rocks were made. The two samples from KAH0204-22 are similar in composition to each other and are essentially duplicate samples. They are granodiorites according to the petrochemical scheme of Middlemost (1994). The third sample, P66839, is granitic (Table 1, 2; Fig. 2B) and has 1.3 wt% corundum in the norm (i.e., it is peraluminous).

A silica versus total alkalies diagram (Fig. 4A) has limitations for metamorphic rocks. However, in overall bulk composition, the granodioritic orthogneisses are somewhat similar to the paragneisses (Fig. 4A,B) but the two sets of gneisses plot on different arrays on an Rb-Sr isochron diagram, the paragneisses being more radiogenic (Fig. 4F). In terms of whole rock geochemistry, possible Northland correlatives of the orthogneisses are the Cretaceous (c. 100 Ma) Houhora Complex (Isaac et al. 1994; Isaac 1996; Nicholson & Black 2004) and the early Miocene (c. 20 Ma) Karikari plutonics (Ruddock 1990; Isaac 1996) which are part of the early Miocene Northland Arc. Alternatively, they could be a new suite of igneous rocks that have no onland equivalent. On a silica versus total alkalies diagram (Fig. 4A), both Houhora and Karikari suites are plausible correlatives for the Cavalli orthogneisses. In terms of trace element contents in the same silica range, the Cavalli orthogneisses have the distinctive high large ion lithophile element content (LILE, e.g., Cs, Rb, Ba, Th, U, K) of the Houhora Complex. Concentrations of high field strength (HFS, e.g., Y, Nb, Zr) and rare-earth elements (REE) are slightly lower and fall between the range of known Houhora Complex and those reported for the Karikari Plutonics. Part of this poor match may result from the fact that there exists a paucity of published trace element data on the Houhora and Northland Arc rocks, and the Cavalli samples number only three. Sr and Nd isotopic data are likewise not distinctive (Fig. 4E), but if the Houhora Complex reference set contained dacites and rhyolites (like that shown for Taupo Volcanic Zone), then a better match might be obtained.

U-Pb dating

Zircon grains were separated from two samples, P66836 biotite paragneiss and P66839 granitic orthogneiss, using standard mineral separation techniques. Before dating, cathodoluminescence images of grains were used to identify target spots on cores and rims where possible. A total of 36 dates were obtained from 29 spot analyses for P66836 and 39 dates from 39 spots for P66839 (Tables 3, 4).

Both samples gave broadly similar results: most of the data fall into two distinct age populations, 20–23 Ma and 98–99 Ma, with scattered intermediate ages and several inherited grains (Fig. 5). For orthogneiss P66839, the principal age populations are 19.7 ± 0.8 Ma (2 σ error, n = 5, MSWD = 2.05) and 98.3 ± 1.6 Ma (2 σ error, n = 13, MSWD = 1.16). For paragneiss P66836, the principal age populations are 22.9 ± 0.6 Ma (2 σ error, n = 7, MSWD = 1.72) and 99.2 ± 1.4 Ma (2 σ error, n = 14, MSWD = 1.31). A large number of grains in the orthogneiss P66839 gave a range of ages intermediate between the two principal age populations. With the relatively low precision of the LA-ICP-MS method, some of these intermediate ages appear concordant (Fig. 5), but $^{208}Pb/^{232}Th$ data indicate they are not. A total of six grains in the paragneiss and one grain in the orthogneiss had $^{206}Pb/^{238}U$ ages of 120–610 Ma, which we interpret as inherited detrital cores. The ages of these inherited grains broadly match those of detrital zircons from the Waipapa Terrane basement of onland Northland (Adams et al. 2007). All spots that yielded early Miocene ages (resolved rims in the case of grains from P66836) have high U concentrations and correspondingly low Th/U ratios compatible with a metamorphic origin (Rubatto 2002; Hoskin & Schaltegger 2003). In contrast, spots with Late Cretaceous ages have U concentrations and Th/U ratios more consistent with an igneous paragenesis.

Ar-Ar and K-Ar dating

K-feldspar is plentiful in the weakly foliated granitic orthogneiss P66839 (Fig. 3D). A step heating experiment reveals an essentially flat plateau from which a very precise age of 19.89 ± 0.05 Ma (2 σ) can be obtained (Fig. 6, Table 5). There is no statistically significant slope on this plateau. Thermal modelling of the spectrum to obtain a 350–150°C time versus temperature cooling curve was not done, as the result would simply be a line parallel to the temperature axis at 19.9 Ma. It is clear that P66839 has cooled exceptionally rapidly for a holocrystalline high grade metaplutonic rock with a 1–2 mm grain size. Taking the error limits literally, this would amount to some 200°C in 100 000 yr for this part of West Cavalli Seamount, a result more than three times the maximum cooling rate inferred for part of East Cavalli by Mortimer et al. (2003). Assuming a geobarometric depth of c. 10 km for the rocks (Mortimer et al. 2003), this converts to a vertical exhumation rate of 100 mm/yr. The Cavalli rocks are thus at the extreme upper limit of known cooling and exhumation rates from a wide range of geological settings (Ring et al. 1999; Dunlap 2000; Rubatto & Herrmann 2001).

Biotite from granodioritic orthogneiss P67674 gave a K-Ar age of 19.3 ± 0.5 Ma (K = 6.72 wt%, $^{40}Ar^*$ = 2.22 × 10^{-10} mol/g, $\%^{40}Ar^*$ = 46.5).

DISCUSSION

Protoliths

Paragneiss

The dominance of zircon grains of c. 100 Ma age with igneous parentage in the paragneiss suggests a strong detrital influence from rocks similar in age to the c. 100 Ma Houhora Complex (Isaac et al. 1994; Isaac 1996). We cannot, on existing data, firmly establish if the protoliths were actually Cretaceous

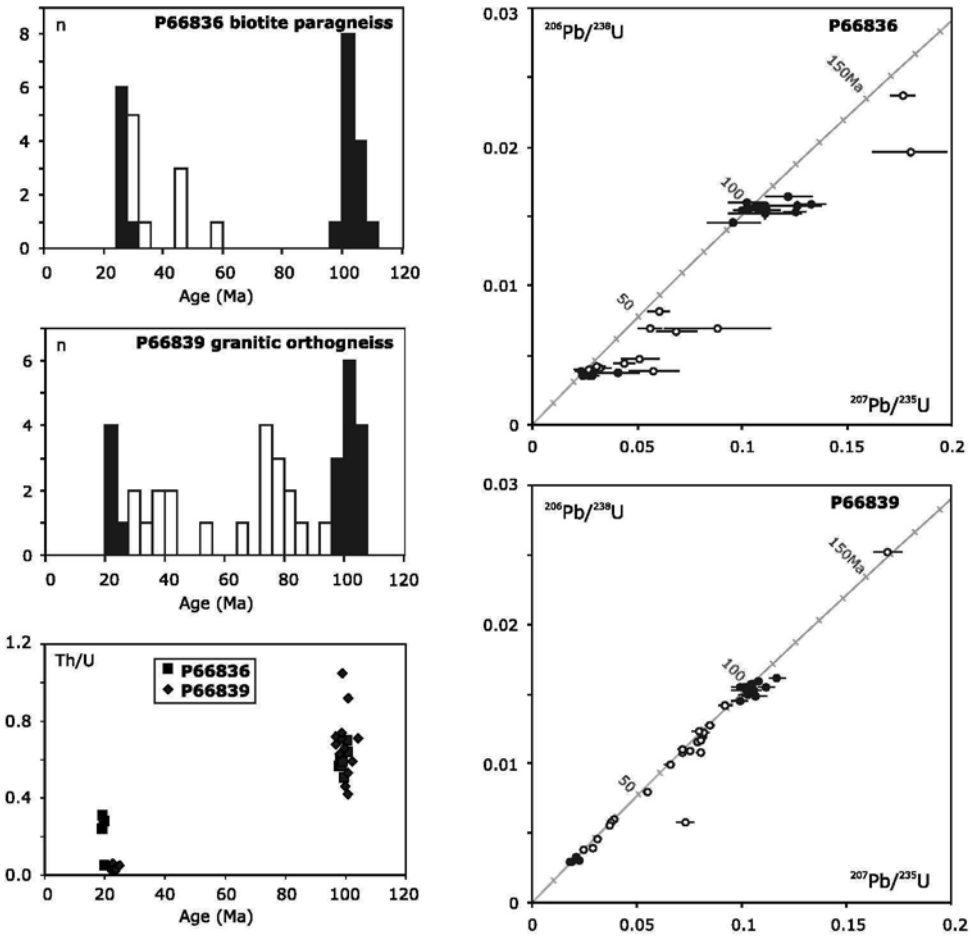

Fig. 5 U-Pb ages and Th/U ratios of zircon grains from garnet biotite paragneiss P66836 and granitic orthogneiss P66839. Black symbols are concordant analyses that gave pooled early Miocene and Late Cretaceous age populations. White symbols are discordant analyses excluded from the early Miocene and Late Cretaceous age populations.

strata or, like the schist dated by Mortimer et al. (2003), probable Cenozoic strata whose detrital mineralogy was derived from local basement (in this case mainly Houhora Complex with minor Waipapa Terrane). If a Cretaceous age for the intruding orthogneisses is accepted (see below) then the West Cavalli paragneiss would indeed have a Cretaceous depositional age.

Orthogneiss

On balance we interpret the geochemical, tracer isotope, and U-Pb zircon data to support a Cretaceous rather than Miocene age of igneous rock formation. Evidence in support of a Cretaceous age is the contrast in Th/U of the zircons (Cretaceous = igneous values, Miocene = metamorphic values, Fig. 5), the high LILE content of the rocks (similar to Houhora Complex, Fig. 4D), and the initial $^{87}Sr/^{86}Sr$ and εNd ratios which should be more similar to the paragneisses if the granite was a Miocene melt from the host rock (Fig. 4E,F). We attribute the imperfect match in the petrochemistry of the Cavalli samples with the onland Houhora samples to (1) aforementioned small datasets, and (2) the presence between onland Northland and Cavalli Seamount of the strike-slip VMFZ. This means that Cavalli Seamount may have originated up to 500 km northwest of its present position (Fig. 7) (Mortimer et al. 2007).

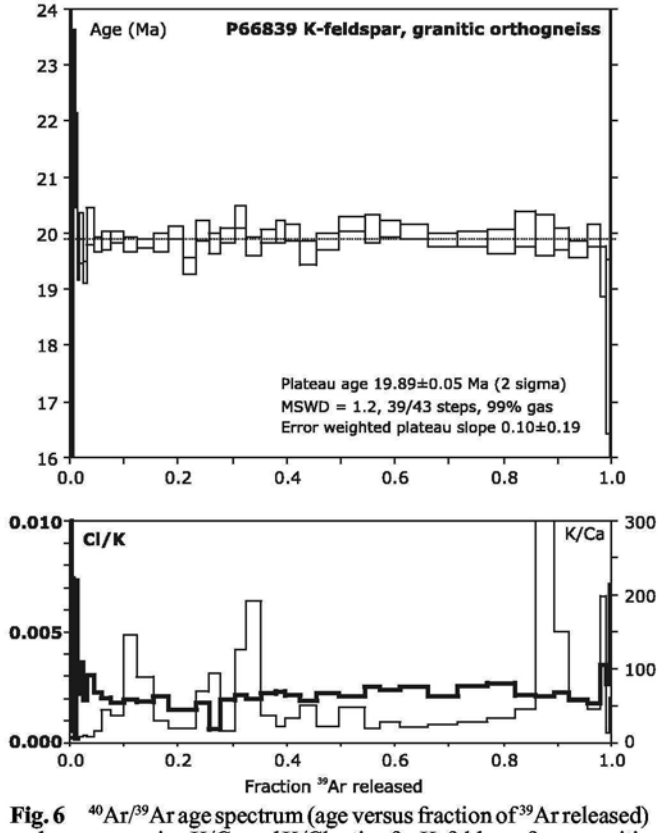

Fig. 6 $^{40}Ar/^{39}Ar$ age spectrum (age versus fraction of ^{39}Ar released) and accompanying K/Ca and K/Cl ratios for K-feldspar from granitic orthogneiss P66839.

Table 3 U-Th-Pb isotope data for Cavalli paragneiss P66836.

Spot	Pb* ppm	U ppm	Th/U atomic	$^{206}Pb/^{238}U$	±1 σ	$^{207}Pb/^{235}U$	±1 σ	$^{207}Pb/^{206}Pb$	±1 σ	$^{208}Pb/^{232}Th$	±1 σ	$^{206}Pb^*/^{238}U$ age (Ma)	±1 σ	$^{206}Pb/^{238}U$ age (Ma)	±1 σ	$^{207}Pb/^{235}U$ age (Ma)	±1 σ	Percent concord	% ^{206}Pb common	Spot MSWD	Age (Ma)	±1 σ
Metamorphic population pooled age (n = 7, MSWD = 1.72, 1 σ absolute external error)																					**22.9**	**0.3**
02-r	11.25	3374	0.04	0.00353	1.5	0.0272	6.9	0.0558	6.7	0.00613	9.0	22.5	0.4	22.7	0.3	27.2	1.9	83	1.16	1.00	22.5	0.4
05-r	8.95	2794	0.02	0.00350	2.1	0.0237	8.1	0.0492	7.9	0.00192	17	22.5	0.5	22.5	0.5	23.8	1.9	95	0.33	1.39	22.5	0.5
01b-r	4.66	1369	0.06	0.00358	2.3	0.0283	13	0.0574	12	0.00462	22	22.7	0.6	23.0	0.5	28.4	3.5	81	1.36	0.76	22.7	0.6
17b-r	4.62	1165	0.03	0.00387	6.0	0.0580	20	0.1088	19	0.03007	13	23.0	1.5	24.9	1.5	57.2	11.3	43	8.30	2.07	23.0	1.5
04-r	3.30	929	0.02	0.00378	5.2	0.0406	25	0.0779	25	0.01597	19	23.4	1.4	24.3	1.3	40.4	10.0	60	4.03	1.09	23.4	1.4
08-r	7.77	2232	0.03	0.00372	2.7	0.0290	13	0.0566	12	0.00737	13	23.6	0.7	23.9	0.6	29.0	3.6	82	1.25	1.88	23.6	0.7
28-r	5.35	1449	0.05	0.00386	3.0	0.0237	12	0.0445	12	0.00606	16	24.9	0.8	24.8	0.7	23.7	2.9	105	–0.25	2.33	24.9	0.8
Igneous population pooled age (n = 14, MSWD = 1.31, 1 σ absolute external error)																					**99.2**	**0.7**
29b-c	2.39	157	0.45	0.01459	2.0	0.0960	13	0.0477	13	0.00481	10	93.4	2.0	93.4	1.9	93.0	11.5	100	–0.02	0.51	93.4	2.0
11	3.66	216	0.68	0.01522	3.2	0.1111	16	0.0530	16	0.00566	6.2	96.8	3.2	97.4	3.1	107.0	16.1	91	0.62	1.61	96.8	3.2
24	4.88	285	0.72	0.01535	1.0	0.1252	4.4	0.0592	4.3	0.00517	2.7	96.8	1.0	98.2	1.0	119.8	5.0	82	1.40	0.84	96.8	1.1
01a-c	9.11	541	0.63	0.01542	1.4	0.1115	6.0	0.0525	5.8	0.00531	5.0	98.1	1.4	98.6	1.4	107.4	6.1	92	0.55	0.66	98.1	1.5
03	7.49	436	0.71	0.01548	1.1	0.1082	4.2	0.0507	4.1	0.00502	2.1	98.7	1.1	99.0	1.1	104.3	4.2	95	0.33	1.51	98.7	1.2
22	9.02	523	0.74	0.01541	0.8	0.0996	4.0	0.0469	4.0	0.00491	2.0	98.7	0.8	98.6	0.8	96.4	3.7	102	–0.13	0.99	98.7	0.9
09	9.45	507	1.05	0.01548	0.9	0.1026	4.2	0.0481	4.1	0.00488	1.5	99.0	0.9	99.0	0.9	99.2	3.9	100	0.01	1.24	99.0	1.0
30	5.46	310	0.66	0.01585	1.0	0.1332	5.4	0.0609	5.3	0.00613	3.0	99.8	1.1	101.4	1.0	127.0	6.4	80	1.61	1.10	99.8	1.2
12a-c	2.41	146	0.46	0.01581	1.6	0.1264	9.0	0.0580	8.9	0.00577	5.0	99.9	1.7	101.1	1.6	120.8	10.3	84	1.23	0.76	99.9	1.8
26a-c	7.58	451	0.53	0.01581	1.5	0.1112	6.4	0.0510	6.2	0.00544	4.1	100.7	1.5	101.1	1.5	107.0	6.5	94	0.37	0.98	100.7	1.6
18a-c	6.73	416	0.42	0.01578	1.6	0.1079	6.4	0.0496	6.2	0.00498	4.2	100.8	1.7	101.0	1.6	104.0	6.3	97	0.19	1.53	100.8	1.7
27a-c	9.14	494	0.92	0.01579	1.2	0.1062	5.1	0.0488	5.0	0.00518	1.9	100.9	1.3	101.0	1.2	102.5	5.0	99	0.09	1.01	100.9	1.3
13	5.25	303	0.59	0.01594	1.8	0.1018	7.9	0.0463	7.7	0.00562	4.1	102.2	1.8	102.0	1.8	98.5	7.4	104	–0.21	1.21	102.2	1.9
15	2.86	158	0.71	0.01639	1.7	0.1220	9.2	0.0540	9.1	0.00520	4.0	104.1	1.8	104.8	1.7	116.9	10.2	90	0.73	0.86	104.1	1.9
Spots showing intermediate dates and/or inheritance																						
19-r	7.66	1994	0.08	0.00394	3.9	0.0270	27	0.0498	27	0.00556	20	25.2	1.1	25.3	1.0	27.1	7.3	94	0.40	1.68	i	
14-r	4.02	1022	0.07	0.00406	2.6	0.0318	19	0.0567	19	0.00604	10	25.8	0.8	26.1	0.7	31.7	5.9	82	1.26	0.53	i	
20-r	7.57	1904	0.07	0.00415	2.8	0.0309	12	0.0541	12	0.00471	20	26.4	0.8	26.7	0.7	30.9	3.7	86	0.94	1.40	i	
18b-r	5.05	1207	0.08	0.00438	5.2	0.0440	12	0.0729	10	0.00470	13	27.3	1.4	28.2	1.5	43.8	5.0	64	3.35	1.57	i	
12b-r	2.65	555	0.10	0.00480	4.3	0.0514	17	0.0778	17	0.00679	37	29.7	1.4	30.8	1.3	50.9	8.6	61	3.99	0.76	i	
27b-r	5.56	772	0.36	0.00670	4.1	0.0688	14	0.0744	14	0.00496	5.7	41.6	1.8	43.0	1.8	67.5	9.3	64	3.51	1.76	i	
26b-r	3.26	477	0.17	0.00696	3.4	0.0882	29	0.0918	29	0.00562	17	42.3	2.0	44.7	1.5	85.8	23.6	52	5.86	0.90	i	
25-r	6.16	901	0.17	0.00691	2.6	0.0560	10	0.0588	9.9	0.00520	8.8	43.7	1.2	44.4	1.1	55.4	5.5	80	1.49	1.71	i	
29a-r	3.48	425	0.20	0.00819	2.0	0.0603	9.4	0.0534	9.2	0.00541	5.4	52.2	1.1	52.6	1.0	59.5	5.4	88	0.79	1.17	i	
17a-c	5.05	235	0.64	0.01963	1.8	0.1801	9.9	0.0665	9.7	0.00707	10	122.6	2.3	125.3	2.2	168.2	15.3	75	2.26	0.54	122.6	2.3
10	9.68	362	0.76	0.02369	0.8	0.1769	3.4	0.0542	3.3	0.00790	1.9	150.0	1.3	150.9	1.2	165.4	5.1	91	0.63	1.21	150.0	1.3
07	4.34	115	0.49	0.03600	1.1	0.2432	5.4	0.0490	5.3	0.01144	3.1	228.5	2.6	228.0	2.5	221.0	10.7	103	–0.21	0.94	228.5	2.6
16	8.25	187	0.72	0.03957	1.9	0.2742	6.3	0.0503	6.0	0.01292	3.0	250.5	4.8	250.2	4.7	246.1	13.7	102	–0.12	1.96	250.5	4.8
06	83.33	1364	0.27	0.05977	11	0.5728	12	0.0695	2.6	0.03769	4.1	367.4	40.6	374.3	41.3	459.8	43.1	81	1.92	994	367.4	40.6
21	59.77	613	0.21	0.09964	0.5	0.8434	1.5	0.0614	1.4	0.03153	1.4	611.5	3.0	612.3	2.9	621.0	6.9	99	0.14	2.21	611.5	3.0

* = radiogenic component only (^{207}Pb-based common-Pb correction), a/b = two ages resolved from progressive drilling of a single zoned single spot, r = rim , c = core analysis where zonation is evident, i = intermediate date of no geological significance.

Table 4 U-Th-Pb isotope data for Cavalli orthogneiss P66839.

Spot	Pb* ppm	U ppm	Th/U atomic	$^{206}Pb/^{238}U$	±1 σ	$^{207}Pb/^{235}U$	±1 σ	$^{207}Pb/^{206}Pb$	±1 σ	$^{208}Pb/^{232}Th$	±1 σ	$^{206}Pb^*/^{238}U$ age (Ma)	±1 σ	$^{206}Pb/^{238}U$ age (Ma)	±1 σ	$^{207}Pb/^{235}U$ age (Ma)	±1 σ	Percent concord	% ^{206}Pb common	Spot MSWD	Age (Ma)	±1 σ
Metamorphic population pooled age (n = 5, MSWD = 2.05, 1 σ absolute external error)																					**19.7**	**0.4**
02	14.65	5052	0.24	0.00296	0.6	0.0184	2.2	0.0450	2.2	0.00102	1.4	19.1	0.1	19.1	0.1	18.5	0.4	103	–0.18	1.77	19.1	0.1
14	18.26	6124	0.31	0.00299	0.5	0.0189	2.0	0.0459	1.9	0.00099	1.6	19.3	0.1	19.2	0.1	19.0	0.4	101	–0.06	1.52	19.3	0.1
20	4.48	1469	0.28	0.00309	0.9	0.0228	4.2	0.0536	4.1	0.00106	3.1	19.7	0.2	19.9	0.2	22.9	0.9	87	0.89	1.23	19.7	0.2
13	1.67	582	0.05	0.00310	1.3	0.0226	5.8	0.0529	5.7	0.00158	9.4	19.8	0.3	20.0	0.3	22.7	1.3	88	0.80	1.07	19.8	0.3
21	3.63	1180	0.07	0.00328	1.0	0.0207	5.1	0.0457	5.0	0.00192	5.3	21.1	0.2	21.1	0.2	20.8	1.1	102	–0.09	1.09	21.1	0.2
Igneous population pooled age (n = 13, MSWD = 1.16, 1 σ absolute external error)																					**98.3**	**0.8**
16	4.89	316	0.53	0.01452	0.8	0.0991	4.0	0.0495	3.9	0.00511	2.1	92.8	0.8	92.9	0.8	95.9	3.6	97	0.20	1.21	92.8	0.8
12-c	11.17	644	0.85	0.01488	1.3	0.1064	5.8	0.0519	5.7	0.00540	2.0	94.8	1.3	95.2	1.3	102.7	5.7	93	0.49	0.97	94.8	1.3
15	4.97	270	1.15	0.01492	1.0	0.1026	3.9	0.0499	3.7	0.00479	1.5	95.3	1.0	95.5	0.9	99.2	3.7	96	0.24	1.50	95.3	1.0
09	10.17	600	0.70	0.01529	0.8	0.1058	3.2	0.0502	3.1	0.00499	1.5	97.5	0.8	97.8	0.8	102.1	3.1	96	0.27	1.59	97.5	0.8
17-c	9.72	595	0.57	0.01530	1.6	0.1022	6.8	0.0485	6.6	0.00475	3.7	97.8	1.6	97.9	1.6	98.8	6.4	99	0.06	1.61	97.8	1.6
36	12.05	711	0.60	0.01546	0.7	0.1115	3.2	0.0523	3.1	0.00589	2.2	98.3	0.7	98.9	0.7	107.3	3.2	92	0.54	1.45	98.3	0.7
26	5.94	360	0.57	0.01548	0.8	0.1119	3.6	0.0524	3.5	0.00497	1.8	98.5	0.8	99.0	0.8	107.7	3.6	92	0.55	1.37	98.5	0.8
37	8.30	499	0.59	0.01547	0.9	0.1024	3.2	0.0480	3.1	0.00494	1.5	99.0	0.9	99.0	0.8	99.0	3.0	100	0.00	2.03	99.0	0.9
06	4.54	277	0.51	0.01553	0.9	0.0995	4.2	0.0465	4.1	0.00497	2.0	99.5	0.9	99.3	0.9	96.3	3.9	103	–0.19	1.26	99.5	0.9
03	13.76	791	0.70	0.01571	0.6	0.1054	2.2	0.0487	2.2	0.00506	1.2	100.4	0.6	100.5	0.6	101.8	2.2	99	0.08	1.57	100.4	0.6
19	7.30	425	0.64	0.01576	0.7	0.1042	3.2	0.0480	3.1	0.00499	1.6	100.8	0.7	100.8	0.7	100.6	3.0	100	–0.01	1.07	100.8	0.7
24	24.04	1319	0.83	0.01595	0.6	0.1078	1.6	0.0490	1.5	0.00507	0.9	101.9	0.6	102.0	0.6	103.9	1.6	98	0.12	2.30	101.9	0.6
23	8.51	417	1.24	0.01610	0.7	0.1168	3.3	0.0526	3.2	0.00547	1.3	102.4	0.8	103.0	0.7	112.2	3.5	92	0.56	1.25	102.4	0.8
Spots showing intermediate dates and/or inheritance																						
34-r	7.95	2201	0.09	0.00376	2.0	0.0244	7.2	0.0471	6.9	0.00326	5.9	24.2	0.5	24.2	0.5	24.5	1.7	99	0.07	1.80	i	
01	4.06	1089	0.12	0.00388	1.1	0.0287	4.4	0.0536	4.3	0.00288	3.7	24.7	0.3	24.9	0.3	28.7	1.3	87	0.88	1.86	i	
31-r	6.69	1489	0.13	0.00460	2.4	0.0314	6.3	0.0495	5.8	0.00385	5.0	29.5	0.7	29.6	0.7	31.4	1.9	94	0.35	1.84	i	
04	4.22	708	0.22	0.00581	2.1	0.0734	6.1	0.0915	5.8	0.00548	6.6	35.3	0.8	37.4	0.8	71.9	4.3	52	5.84	4.25	i	
29	9.81	1620	0.38	0.00552	0.9	0.0367	2.9	0.0483	2.7	0.00411	1.5	35.4	0.3	35.5	0.3	36.6	1.0	97	0.19	2.76	i	
10	14.10	2406	0.24	0.00579	0.9	0.0379	2.7	0.0475	2.5	0.00357	1.9	37.2	0.3	37.2	0.3	37.8	1.0	99	0.09	2.04	i	
08	11.45	1930	0.18	0.00597	0.8	0.0394	3.2	0.0478	3.1	0.00421	1.6	38.3	0.3	38.4	0.3	39.2	1.2	98	0.13	3.09	i	
18	11.02	1407	0.22	0.00799	2.9	0.0549	4.0	0.0498	2.7	0.00351	2.9	51.1	1.5	51.3	1.5	54.3	2.1	95	0.34	33.52	i	
22	9.11	860	0.45	0.00996	2.4	0.0657	3.8	0.0479	2.9	0.00433	1.7	63.8	1.5	63.9	1.5	64.7	2.4	99	0.07	19.67	i	
07	12.55	1066	0.53	0.01082	1.4	0.0804	2.8	0.0539	2.4	0.00481	1.4	68.8	1.0	69.4	1.0	78.5	2.1	88	0.80	8.83	i	
11	17.28	1481	0.52	0.01079	0.8	0.0719	2.5	0.0483	2.4	0.00450	1.4	69.1	0.6	69.2	0.6	70.5	1.7	98	0.11	1.85	i	
39	13.72	1175	0.50	0.01094	1.3	0.0754	2.6	0.0500	2.2	0.00440	1.1	70.0	0.9	70.2	0.9	73.9	1.8	95	0.32	6.02	i	
32	11.45	818	1.17	0.01100	0.9	0.0718	3.4	0.0473	3.3	0.00421	1.3	70.5	0.6	70.5	0.6	70.4	2.3	100	–0.01	1.68	i	
30	28.60	2227	0.65	0.01153	1.2	0.0788	2.0	0.0496	1.6	0.00454	1.0	73.7	0.9	73.9	0.9	77.0	1.5	96	0.26	11.83	i	
38	12.04	926	0.68	0.01172	0.8	0.0803	3.3	0.0497	3.2	0.00415	1.3	74.9	0.6	75.1	0.6	78.4	2.5	96	0.27	1.53	i	
28	10.68	804	0.68	0.01188	0.8	0.0814	2.7	0.0497	2.6	0.00444	1.6	75.9	0.6	76.1	0.6	79.5	2.0	96	0.27	2.26	i	
33	15.29	1003	1.12	0.01225	0.8	0.0819	3.4	0.0485	3.3	0.00437	1.2	78.4	0.6	78.5	0.6	79.9	2.6	98	0.11	1.63	i	
40	4.22	328	0.44	0.01234	1.5	0.0797	4.8	0.0468	4.6	0.00466	2.1	79.2	1.2	79.1	1.2	77.9	3.6	102	–0.09	3.13	i	
25	11.95	829	0.71	0.01276	0.9	0.0849	2.7	0.0483	2.5	0.00472	1.3	81.7	0.7	81.7	0.7	82.8	2.1	99	0.08	2.98	i	
35	22.26	1152	1.59	0.01420	0.8	0.0921	3.4	0.0471	3.3	0.00451	1.3	91.0	0.8	90.9	0.8	89.5	3.0	102	–0.09	1.29	i	
27-c	12.64	388	1.34	0.02520	0.6	0.1696	4.0	0.0488	4.0	0.00812	1.5	160.5	1.1	160.5	1.0	159.1	5.9	101	–0.05	0.62	160.5	1.1

* = radiogenic component only (^{207}Pb-based common-Pb correction), r = rim , c = core analysis where zonation is evident, i = intermediate date of no geological significance.

Table 5 Ar-Ar data for K-feldspar from P66839. λ^{40} K = 5.5430E-10, J = 2.9195E-4.

T (°C)	^{36}Ar (mol)	^{37}Ar (mol)	^{38}Ar (mol)	^{39}Ar (mol)	^{40}Ar (mol)	%^{40}Ar*	^{40}Ar*/^{39}Ar(K)	Cum ^{39}Ar	Age	±	1 σ	Ca/K	Cl/K
450	9.853E-16	3.033E-17	3.228E-16	3.404E-16	3.169E-13	8.1	75.79	0.1	39.48	±	8.24	1.69E-01	3.43E-02
450	1.249E-16	8.530E-17	1.732E-16	1.311E-15	3.842E-14	3.9	1.144	0.7	0.60	±	1.81	1.24E-01	5.33E-04
500	1.676E-16	1.557E-17	9.911E-17	3.575E-16	6.434E-14	23.0	41.42	0.9	21.69	±	1.72	8.28E-02	7.39E-03
500	1.043E-16	6.029E-17	9.165E-17	4.146E-16	4.877E-14	36.8	43.27	1.0	22.64	±	0.98	2.76E-01	5.47E-03
550	2.603E-16	2.410E-18	2.138E-16	8.740E-16	1.125E-13	31.6	40.68	1.4	21.30	±	0.84	5.24E-03	7.33E-03
550	6.069E-17	1.226E-16	1.463E-16	9.125E-16	5.205E-14	65.5	37.39	1.8	19.59	±	0.43	2.55E-01	2.23E-03
600	2.255E-16	9.073E-17	2.880E-16	1.542E-15	1.253E-13	46.8	38.02	2.4	19.92	±	0.45	1.12E-01	3.66E-03
600	5.624E-17	9.602E-17	2.675E-16	1.767E-15	8.170E-14	79.6	36.83	3.2	19.29	±	0.20	1.03E-01	1.93E-03
650	2.059E-16	1.578E-16	4.455E-16	2.634E-15	1.622E-13	62.5	38.45	4.3	20.14	±	0.34	1.14E-01	3.05E-03
650	5.305E-17	1.095E-16	5.099E-16	3.374E-15	1.433E-13	89.0	37.81	5.8	19.81	±	0.14	6.17E-02	2.27E-03
700	1.830E-16	5.105E-17	6.735E-16	4.370E-15	2.199E-13	75.4	37.92	7.6	19.86	±	0.16	2.22E-02	2.03E-03
700	3.972E-17	7.937E-17	8.099E-16	5.555E-15	2.233E-13	94.7	38.08	10.0	19.95	±	0.10	2.71E-02	1.81E-03
750	1.231E-16	2.092E-17	8.690E-16	5.809E-15	2.561E-13	85.7	37.80	12.4	19.80	±	0.14	6.84E-03	1.95E-03
750	4.144E-17	4.203E-17	1.035E-15	7.087E-15	2.804E-13	95.6	37.82	15.4	19.81	±	0.08	1.13E-02	1.86E-03
800	1.360E-16	1.085E-16	9.398E-16	6.225E-15	2.759E-13	85.4	37.85	18.1	19.83	±	0.16	3.31E-02	2.11E-03
800	4.437E-17	1.782E-16	9.863E-16	6.898E-15	2.767E-13	95.2	38.20	21.0	20.01	±	0.12	4.91E-02	1.47E-03
850	1.455E-16	1.359E-16	7.690E-16	5.221E-15	2.366E-13	81.8	37.06	23.2	19.41	±	0.16	4.95E-02	1.51E-03
850	6.505E-17	4.440E-17	8.667E-16	5.905E-15	2.453E-13	92.1	38.26	25.8	20.04	±	0.18	1.43E-02	1.84E-03
900	1.751E-16	2.739E-17	6.939E-16	4.894E-15	2.370E-13	78.1	37.83	27.8	19.82	±	0.18	1.06E-02	6.34E-04
900	9.178E-17	2.036E-16	9.135E-16	6.165E-15	2.624E-13	89.6	38.15	30.4	19.98	±	0.13	6.28E-02	1.92E-03
950	1.856E-16	2.104E-17	7.755E-16	5.030E-15	2.499E-13	78.0	38.76	32.6	20.30	±	0.20	7.95E-03	2.15E-03
950	1.666E-16	1.686E-17	9.270E-16	6.138E-15	2.809E-13	82.4	37.73	35.2	19.76	±	0.16	5.22E-03	1.99E-03
950	2.524E-16	9.641E-17	1.049E-15	6.767E-15	3.325E-13	77.5	38.09	38.1	19.95	±	0.12	2.71E-02	2.25E-03
1000	2.878E-16	9.832E-17	6.595E-16	4.074E-15	2.409E-13	64.7	38.23	39.8	20.02	±	0.20	4.59E-02	2.32E-03
1000	2.847E-16	9.711E-17	9.552E-16	6.126E-15	3.184E-13	73.5	38.22	42.4	20.02	±	0.16	3.01E-02	2.15E-03
1050	4.791E-16	7.605E-17	1.147E-15	7.271E-15	4.145E-13	65.8	37.51	45.5	19.65	±	0.21	1.99E-02	1.92E-03
1050	4.380E-16	2.335E-16	1.558E-15	9.986E-15	5.082E-13	74.5	37.92	49.7	19.86	±	0.14	4.44E-02	2.23E-03
1050	3.958E-16	1.203E-16	1.686E-15	1.096E-14	5.391E-13	78.3	38.48	54.4	20.16	±	0.14	2.08E-02	2.12E-03
1100	2.983E-16	1.685E-16	1.020E-15	6.423E-15	3.345E-13	73.6	38.35	57.1	20.09	±	0.24	4.98E-02	2.51E-03
1100	2.994E-16	1.742E-16	1.457E-15	9.397E-15	4.490E-13	80.3	38.35	61.1	20.09	±	0.16	3.52E-02	2.39E-03
1100	3.629E-16	2.965E-16	1.862E-15	1.193E-14	5.638E-13	80.9	38.25	66.2	20.03	±	0.13	4.72E-02	2.54E-0
1100	4.463E-16	2.786E-16	1.997E-15	1.303E-14	6.266E-13	78.9	37.96	71.7	19.88	±	0.11	4.06E-02	2.10E-03
1100	5.234E-16	2.269E-16	1.950E-15	1.231E-14	6.226E-13	75.1	38.00	77.0	19.90	±	0.13	3.50E-02	2.56E-03
1100	6.819E-16	1.926E-16	1.999E-15	1.234E-14	6.692E-13	69.9	37.87	82.2	19.84	±	0.21	2.97E-02	2.69E-03
1100	8.628E-16	1.034E-16	1.473E-15	8.904E-15	5.967E-13	57.2	38.36	86.0	20.09	±	0.31	2.21E-02	2.15E-03
1100	1.520E-15	2.700E-19	1.512E-15	8.354E-15	7.677E-13	41.5	38.13	89.5	19.97	±	0.37	6.14E-05	2.10E-03
1200	5.165E-16	2.127E-17	9.964E-16	6.069E-15	3.833E-13	60.2	37.99	92.1	19.90	±	0.20	6.66E-03	2.27E-03
1230	1.708E-16	7.225E-17	1.159E-15	7.738E-15	3.420E-13	85.2	37.66	95.4	19.72	±	0.15	1.77E-02	1.96E-03
1260	1.537E-16	7.041E-17	9.203E-16	6.179E-15	2.810E-13	83.8	38.12	98.0	19.96	±	0.20	2.17E-02	1.78E-03
1290	1.223E-16	6.911E-18	4.344E-16	2.605E-15	1.322E-13	72.6	36.87	99.1	19.32	±	0.44	5.04E-03	3.49E-03
1320	1.694E-16	3.722E-17	1.805E-16	9.846E-16	8.384E-14	40.3	34.30	99.5	17.98	±	1.55	7.18E-02	2.63E-03
1350	3.118E-16	1.498E-17	1.248E-16	4.112E-16	1.081E-13	14.7	38.71	99.7	20.27	±	4.84	6.92E-02	3.87E-03
1450	4.313E-15	5.773E-18	9.353E-16	6.672E-16	1.301E-12	2.0	39.22	100.0	20.54	±	23.78	1.64E-02	7.11E-03
Total	1.653E-14	4.091E-15	3.789E-14	2.354E-13	1.380E-11		37.88		19.84	±	0.29		

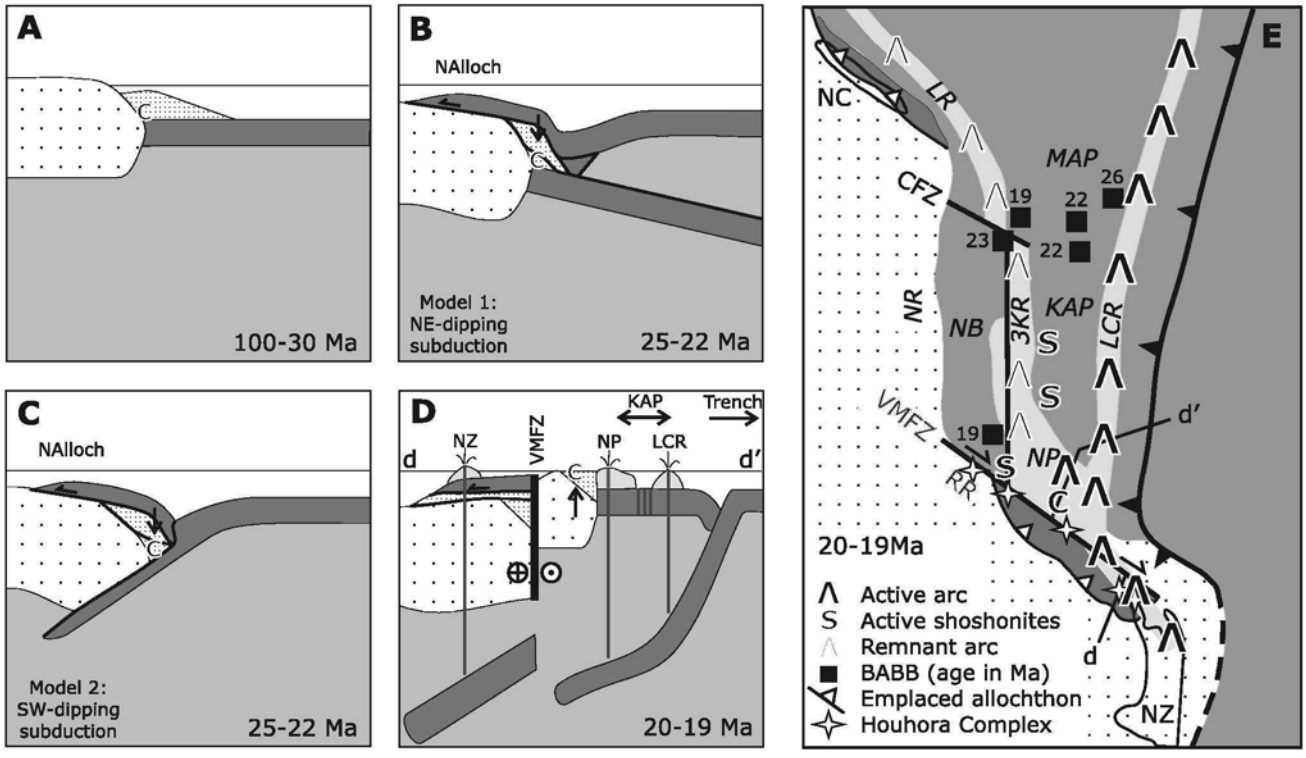

Fig. 7 Schematic cross-sections and map showing tectonic context of Cavalli Seamount (C) in the Oligocene–Miocene. Cross-sections are based on Malpas et al. (1992) and oriented approximately northeast–southwest across the continental margin between New Zealand (NZ) and the Reinga Ridge (RR). Arrows emphasise significant vertical and horizontal motion. **A**, Late Cretaceous Cavalli protoliths deposited near bottom of sediment wedge on older Mesozoic orogen. **B**, Northeast-dipping subduction model for Northland Allochthon emplacement. **C**, Southwest-dipping subduction model for Northland Allochthon emplacement. **D**, Rapid post-allochthon, early Miocene exhumation to sea level of Cavalli Seamount can be related to dextral (and possibly transtensional) strike-slip movement on the Vening Meinesz Fracture Zone (VMFZ), Pacific trench rollback, an opening Kupe Abyssal Plain back-arc basin, and widespread subduction-related volcanism and shoshonitic rift-related volcanism. Twin subducted slabs are derived from different along-strike portions of the same Pacific slab on different sides of the VMFZ. Cross-section line d–d′ is offset on VMFZ. **E**, Map view showing features described in panel D. NZ = New Zealand, NC = New Caledonia, NP = Northland Plateau, VMFZ = Vening Meinesz Fracture Zone, CFZ = Cook Fracture Zone, NB = Norfolk Basin, MAP = Minerva Abyssal Plain, KAP = Kupe Abyssal Plain, NR = Norfolk Ridge, 3KR = Three Kings Ridge, TKR = Tong-Kermadec Ridge, LR = Loyalty Ridge, BABB = back-arc basin basalt dredge site.

We interpret the dated orthogneiss sample and smaller granitic veins (Table 1) to have been parts of subvolcanic dikes and plutons that intruded a Late Cretaceous silicic volcanic-volcaniclastic carapace, similar to the case of the Houhora Complex (Isaac et al. 1994; Isaac 1996). As such, the broad similarity between orthogneisses and paragneiss bulk rock compositions need not be coincidence. We do not entirely rule out some remobilisation and/or migmatisation of the Cretaceous protoliths in the early Miocene (e.g., at the time of intrusion of the Karikari Plutonics).

Metamorphism and exhumation

Mortimer et al. (2003) were unable to constrain the age of prograde amphibolite facies metamorphism of the schists and gneisses. The new U-Pb data presented in Fig. 5 indicate metamorphic zircon growth possibly as early as 23 Ma and possibly as late as 20 Ma. This definitely seems to link the prograde metamorphism with other early Miocene events in onland and offshore Northland (Mortimer et al. 2003, 2007), rather than to some Cretaceous or Paleogene event. The Ar-Ar dating of a single separate of K-feldspar from West Cavalli (P66839) provides a simpler and less ambiguous cooling history than the multiple minerals and methods used by Mortimer et al. (2003) for the East Cavalli dredge site. P66839 underwent exceptionally rapid cooling rates of c. 2000°C/Ma through the 350–150°C temperature range at 19.9 Ma. The cooling interval of 23–21 Ma cited by Mortimer et al. (2003) was arrived at by the need to accommodate a 25 ± 4 Ma zircon fission track age. While different parts of Cavalli may have been exhumed at different times (the 1999 and 2002 sample sites are 20 km apart), the current study would appear to provide a more precise and consistent result, with which all thermochronological and micropaleontological data of Mortimer et al. (2003), except the zircon fission track age, are entirely compatible. The inferred vertical exhumation rate of c. 100 mm/yr is comparable to moderately fast horizontal plate tectonic rates and matches the inferred 67–100 mm/yr rate calculated for the VMFZ from the alignment of Kupe Abyssal Plain hotspot tracks (Mortimer et al. 2007).

Tectonic model

From the combined results of the 1999 and 2002 dredges, Cavalli Seamount protoliths are now known to consist of correlatives of Late Cretaceous–Paleogene sedimentary cover derived from Waipapa Terrane (Mortimer et al. 2003) and also Late Cretaceous sedimentary and plutonic rocks similar to Houhora Complex (this study) (Fig. 7A). Both these rock units are present in autochthonous basement of present day onland

Northland, although the Cavalli rocks may actually have been ripped off the continental Reinga Ridge many hundreds of kilometres to the northwest where Houhora-like rocks are known to occur (Mortimer et al. 1998). This arises as a simple consequence of the position of Cavalli Seamount oceanward of the VMFZ (Fig. 1), and of closing the Norfolk Basin, and perhaps parts of Kupe Abyssal Plain, along the VMFZ (Fig. 7) (Herzer & Mascle 1996; Mortimer et al. 2007).

The Northland Allochthon was emplaced in the interval 25–22 Ma, thus it is plausible to associate the 23–20 Ma Cavalli high grade metamorphism with crustal thickening associated with allochthon emplacement, similar to models of Eocene allochthon emplacement and metamorphism in New Caledonia (Cluzel et al. 2001; Crawford et al. 2003). The recovery of plutonic and metamorphic rocks of similar, amphibolite facies, metamorphic grade from a wide area on Cavalli Seamount (Fig. 2) would seem to argue against the rocks occurring as a thin sub-allochthon metamorphic sole (one option considered by Mortimer et al. 2003) but would suggest a distribution throughout a more significant crustal volume. Two different scenarios for tectonic burial of the Cavalli rocks to amphibolite facies depths in thickened crust beneath the Northland Allochthon are presented in Fig. 7B,C (after Malpas et al. 1992). Neither the present study, nor that of Mortimer et al. (2007), is able to provide a test of the polarity of emplacement of the Northland Allochthon.

The early Miocene was a time of intense tectonomagmatic activity and change in and near northern New Zealand. Mortimer et al. (2007) attributed this to tandem opening of the Norfolk and Kupe back-arc basins behind a rapidly east-retreating Pacific trench, separated from the continental crust of Zealandia by the VMFZ (Fig. 7D,E). Between the southern Norfolk Basin and offshore Northland, the VMFZ is known to be a major dextral strike-slip fault system (Isaac et al. 1994; Herzer & Mascle 1996).

The exhumation event in which Cavalli schists and gneisses came from c. 10 km depth to exposure and planation at sea level by the Altonian (19–17 Ma) (Mortimer et al. 2003) is now more accurately and precisely dated at 19.9 Ma and inferred to have had an exceptional vertical exhumation rate of c. 100 mm/yr. Exhumation clearly followed the 25–22 Ma emplacement of the Northland Allochthon. The images of stretching lineations and sediment-filled cracks (Fig. 3A,B) provide outcrop information that was unavailable to Mortimer et al. (2003) that also can be fitted into a model. Unfortunately, we do not know if the Cavalli rocks are part of a longer linear belt, or are a unique point occurrence.

Mortimer et al. (2003) noted that the rapid early Miocene exhumation of Cavalli Seamount was consistent with it being in the lower plate of an early Miocene metamorphic core complex. Our new data still support this conclusion but we can now better identify the tectonic controls on exhumation. Fast rates of vertical exhumation of metamorphic rocks have been associated with extensional metamorphic core complexes where oceanic spreading ridges propagate into continental borderlands (e.g., >10 mm/yr exhumation rate, Baldwin et al. 2004), with continent-continent collision zones (e.g., 34 mm/yr, Rubatto & Hermann 2001; 6–9 mm/yr, Little et al. 2005) and in complex back-arc basin settings (e.g., >4 mm/yr, Thomson et al. 1998; Ring & Reishmann 2002). Core complex formation and exhumation has also been described from intracontinental strike-slip regimes (e.g., Whitney et al. 2007). Although the 10 km paleodepth estimates for the Cavalli gneisses is not well constrained, the inferred exhumation rate far exceeds the aforementioned estimates which are generally considered to be fast (see also Ring et al. 1999). We believe that the extreme Cavalli exhumation rate is a result of the coincidence in space and time of multiple tectonic conditions favouring local vertical motion. Contributing factors to the rapid exhumation were probably: (1) up to 100 mm/yr dextral motion on the adjacent VMFZ; (2) rapid Pacific trench rollback; (3) possible soft link to a coeval rapid back-arc spreading in the Kupe Abyssal Plain; and (4) buoyancy-assisted uplift of an overthickened continental crust fragment against the VMFZ.

Figure 7D,E shows Cavalli Seamount in this regional context of dextral transform faulting with subduction- and rift-related volcanoes erupting on both sides of the VMFZ. Improved understanding of the regional kinematic significance of Cavalli Seamount must await seismic surveys of the Northland continental margin to better define controlling structures, and local multibeam bathymetric mapping of Cavalli Seamount to enable matching of our hand sample and outcrop scale data with regional scale fault patterns.

CONCLUSIONS

Two cruises to Cavalli Seamount in 2002 added to the material obtained on an earlier cruise in 1999 (Mortimer et al. 2003). The 2002 cruises yielded outcrop photographs, more samples of high grade metasedimentary rocks, and, for the first time, metaplutonic rocks. Our analytical work indicates that Late Cretaceous protoliths similar to Houhora Complex are present on West Cavalli, as well as the previously established Waipapa Terrane-derived sedimentary cover rocks on East Cavalli. U-Pb dating of zircons indicates amphibolite facies (sillimanite grade) metamorphism to have taken place in the interval 20–23 Ma, and is plausibly related to crustal thickening associated with emplacement of the Northland Allochthon. Ar-Ar dating of K-feldspar indicates that ultra-fast exhumation took place at 19.9 Ma. Extremely rapid mid-crustal exhumation took place in a regime of intra-arc dextral transtension between the VMFZ and a retreating Pacific trench.

ACKNOWLEDGMENTS

We are grateful to the Captain and crew of the RVs *Tangaroa* and *Kaharoa* for successful cruises in 2002. Neville Orr, John Simes, Belinda Smith Lyttle, and John Hunt provided their usual high quality technical support. Comments from two anonymous referees helped improve the content of the paper. We also thank the Australian Institute of Nuclear Science and Engineering (AINSE) and the Australian Nuclear Science Technology Organisation (ANSTO) for facilitating irradiation of samples. Funded by the New Zealand Foundation for Research Science and Technology (FRST) Contract CO5X0703 (Physical Resources of the Oceans programme). NIWA's cruise was funded by FRST Contract CO1X0508 (Seamount Biodiversity and Processes).

REFERENCES

Adams CJ, Pankhurst RJ, Maas R, Millar IL 2005. Nd and Sr isotopic signatures of metasedimentary rocks around the South Pacific margin and implications for their provenance. Geological Society of London Special Publication 246: 113–141.

Adams CJ, Campbell HJ, Griffin WL 2007. Provenance comparisons of Permian to Jurassic tectonostratigraphic terranes in New Zealand: perspectives from detrital zircon age patterns. Geological Magazine 144: 701–729.

Baldwin SL, Monteleone BD, Webb LE, Fitzgerald PG, Grove M, Hill EJ 2004. Pliocene eclogite exhumation at plate tectonic rates in eastern Papua New Guinea. Nature 431: 263–267.

Clark M, Downing K, O'Shea S, Thomas C 2002. Voyage report of a survey of seamounts off the northeast coast of the North Island (KAH0204). Wellington, National Institute of Water and Atmospheric Research. 11 p.

Cluzel D, Aitchison JC, Picard C 2001. Tectonic accretion and underplating of mafic terranes in the late Eocene intraoceanic forearc of New Caledonia (Southwest Pacific): geodynamic implications. Tectonophysics 340: 23–59.

Compton RR 1985. Geology in the field. New York, John Wiley & Sons.

Crawford AJ, Meffre S, Symonds PA 2003. 120 to 0 Ma tectonic evolution of the southwest Pacific and analogous geological evolution of the 600 to 220 Ma Tasman Fold Belt System. Geological Society of America Special Paper 372: 383–403.

Dunlap WJ 2000. Nature's diffusion experiment: the cooling-rate cooling-age correlation. Geology 28: 139–142.

Dunlap WJ 2003. Crystallization versus cooling ages of white micas: dramatic effect of K-poor inclusions on $^{40}Ar/^{39}Ar$ age spectra. Journal of the Virtual Explorer 13, Paper 3.

Herzer RH, Mascle J 1996. Anatomy of a continent-backarc transform—the Vening Meinesz Fracture Zone northwest of New Zealand. Marine Geophysical Research 18: 401–427.

Herzer RH, Mascle J, Davy B, Ruellan E, Mortimer N, Laporte C, Duxfield A 2000. New constraints on the New Zealand–South Fiji Basin continent-back-arc margin. Comptes Rendu de l'Académie des Sciences, Paris, Sciences de la Terre et des Planètes 330: 701–708.

Herzer RH, Davy B, Mortimer N, Laporte-Magoni C, Barker D 2004. Cruise report—GNS Cruise SF0202 "ONSIDE II" (Offshore Northland Seismic and Dredging Expedition II). Institute of Geological & Nuclear Sciences File Report 2004-01.

Hoskin PWO, Schaltegger U 2003. The composition of zircon and igneous and metamorphic petrogenesis. Reviews in Mineralogy and Geochemistry 53: 27–62.

Isaac MJ comp. 1996. Geology of the Kaitaia area. Institute of Geological & Nuclear Sciences 1:250 000 Geological Map 1. Lower Hutt, New Zealand, Institute of Geological & Nuclear Sciences Ltd.

Isaac MJ, Herzer RH, Brook FJ, Hayward BW 1994. Cretaceous and Cenozoic sedimentary basins of Northland, New Zealand. Institute of Geological & Nuclear Sciences Monograph 8.

Little TA, Cox S, Vry JK, Batt G 2005. Variations in exhumation level and uplift rate along the oblique-slip Alpine fault, central Southern Alps, New Zealand. Geological Society of America Bulletin 117: 707–723.

Malpas J, Spörli KB, Black PM, Smith IEM 1992. Northland ophiolite, New Zealand, and implications for plate-tectonic evolution of the southwest Pacific. Geology 20: 149–152.

McCulloch MT, Kyser TK, Woodhead JD, Kinsley K 1994. Pb-Sr-Nd-O isotopic constraints on the origin of rhyolites from the Taupo Volcanic Zone of New Zealand: evidence for assimilation followed by fractionation from basalt. Contributions to Mineralogy and Petrology 115: 303–312.

Middlemost EAK 1994. Naming materials in the magma/igneous rock system. Earth Science Reviews 37: 215–224.

Mitchell JS, Eade JV 1990. North Cape bathymetry. New Zealand Oceanographic Institute Chart, coastal series, 1:200 000.

Mortimer N, Herzer RH, Gans PB, Parkinson DL, Seward D 1998. Basement geology from Three Kings Ridge to West Norfolk Ridge, southwest Pacific Ocean: evidence from petrology, geochemistry and isotopic dating of dredge samples. Marine Geology 148: 135–162.

Mortimer N, Herzer RH, Walker NW, Calvert AT, Seward D, Chaproniere GCH 2003. Cavalli Seamount, Northland Plateau, SW Pacific Ocean: a Miocene metamorphic core complex? Journal of the Geological Society (London) 160: 971–983.

Mortimer N, Hoernle K, Hauff F, Palin JM, Dunlap WJ, Werner R, Faure K 2006. New constraints on the age and evolution of the Wishbone Ridge, southwest Pacific Cretaceous microplates, and Zealandia-West Antarctica breakup. Geology 34: 185–189.

Mortimer N, Herzer RH, Gans PB, Laporte-Magoni C, Calvert AT, Bosch D 2007. Oligocene-Miocene tectonic evolution of the South Fiji Basin and Northland Plateau, SW Pacific Ocean: evidence from petrology and dating of dredged rocks. Marine Geology 237: 1–24.

Nicholson KN, Black PM 2004. Cretaceous to early Tertiary basaltic volcanism in the Far North of New Zealand: geochemical associations and their tectonic significance. New Zealand Journal of Geology and Geophysics 47: 437–446.

Nicholson KN, Black PM, Picard C 2000. Geochemistry and tectonic significance of the Tangihua Ophiolite Complex, New Zealand. Tectonophysics 321: 1–15.

Palmer K, Mortimer N, Nathan S, Isaac MJ, Field BD, Sircombe KN, Black PM, Bush S, Orr NW 1995. Chemical and petrographic analyses of some New Zealand Paleozoic–Mesozoic metasedimentary and igneous rocks. Institute of Geological & Nuclear Sciences Science Report 95/16. 37 p.

Ring U, Reishmann T 2002. The weak and superfast Cretan detachment, Greece: exhumation at subduction rates in extruding wedges. Journal of the Geological Society (London) 159: 225–228.

Ring U, Brandon MT, Willett SD, Lister GS 1999. Exhumation processes. Geological Society of London Special Publication 154: 1–27.

Rubatto D 2002. Zircon trace element geochemistry: partitioning with garnet and the link between U-Pb ages and metamorphism. Chemical Geology 184: 123–138.

Rubatto D, Herrmann J 2001. Exhumation as fast as subduction? Geology 29: 3–6.

Ruddock RS 1990. The Karikari Plutonics of Northland, New Zealand. Unpublished PhD thesis, University of Auckland, Auckland, New Zealand.

Spell TL, McDougall I 2003. Characterization and calibration of $^{40}Ar/^{39}Ar$ dating standards. Chemical Geology 198: 189–211.

Sun SS, McDonough WF 1989. Chemical and isotopic systematics of oceanic basalts: implications for mantle compositions and processes. Geological Society of London Special Publication 42: 313–345.

Thomson SN, Stöckhert B, Brix MA 1998. Thermochronology of the high-pressure metamorphic rocks of Crete, Greece: implications for the speed of tectonic processes. Geology 26: 259–262.

Whalen JB, Currie KL, Chappell BW 1987. A-type granites: geochemical characteristics, discrimination and petrogenesis. Contributions to Mineralogy and Petrology 95: 407–419.

Whitney DL, Teyssier C, Heizler MT 2007. Gneiss domes, metamorphic core complexes, and wrench zones: thermal and structural evolution of the Nigde Massif, central Anatolia. Tectonics 26. TC5002, doi:10.1029/2006TC002040.